# Hydrogen Reduction of High Temperature Sintered and Self-Hardened Pellets of Bauxite Residue produced via the Addition of Limestone and Quicklime

**Manish Kumar Kar[1], Casper van der Eijk [2] and Jafar Safarian[3]**
1. Ph.D. Student
3. Associate Professor
Department of Materials Science and Engineering, NTNU, Trondheim, Norway
2. Senior Research Scientist
SINTEF, Trondheim, Norway
Corresponding author: manish.k.kar@ntnu.no

## Abstract

The reduction of iron oxide by hydrogen and phase transformation in Bauxite Residue (BR) were experimentally studied at 1000 °C. In the present work, two types of oxide pellets were first made from bauxite residue via the addition of $CaCO_3$ (Limestone) and CaO (quicklime) powder. The Ca was added to form a leachable mayenite phase ($12CaO.7Al_2O_3$) with the existing alumina in BR. Either only $CaCO_3$ was added or a mixture of CaO and $CaCO_3$ was added (Fixed Ca content). The former was sintered at 1150 ˚C, while the latter could be self-hardened through the cementing effect of CaO in exposure to moisture and air. Both types of pellets were reduced by hydrogen in a thermogravimetry furnace at elevated temperature under similar conditions. The pellets were characterised by X-Ray Diffraction (XRD), Scanning Electron Microscope (SEM) coupled with energy dispersive spectroscopy (EDS), physical and mechanical testing. It was found that the phase formation after reduction is dependent on the characteristics of the used pellets. The high-temperature sintered pellets had higher strength and it was also found that produced oxide pellets were different with respect to the dominant phases present in them. There was a negligible amount of gehlenite ($Ca_2Al_2SiO_7$) formation in the self-hardened pellets, while this phase was a dominant phase in the sintered pellets. The two pellets showed similar reduction behaviour, while different chemical, physical and mechanical properties were observed. Higher iron recovery was observed in the reduced sintered pellets. On the other hand, the reduced self-hardened pellets had a higher amount of alumina containing mayenite leachable phase.

**Keywords:** Hydrogen reduction, Bauxite residue, Thermogravimetry, Self-hardened pellet, Sintered pellet, Phase transformation.

## 1. Introduction

As the modernization of society is growing, the demand for aluminium has increased with time [1]. Bauxite is the major raw material for the production of alumina. Most alumina is produced around the world through the Bayer's process, which generates a waste known as red mud or bauxite residue(BR) in dewatered form [2]. However, the generation of BR has serious environmental challenges due to its properties and challenges to storage [2]. Many researchers have tried to find an efficient way of the utilization of BR because it can be a potential secondary source for the metals like Fe, Al, Ti, Ca, and many more. However, utilization of BR is still impenetrable mainly due to economic reasons and running efficient processes. That is why it is important to find out a different technology for the utilization of BR to get rid of the environmental problem[3]. As the environmental greenhouse gas concern increases with time, green reduction will be a promising technology for the oxide reduction in BR.

Most of the iron production in the world is through the blast furnace and basic oxygen furnace (BF/BOF) route, which needs coking coal both as a reductant and heat source. As the shortage of

coking coal increases and the environmental climate concern increases, hydrogen will most likely be the future reductant for the steel industry [4]. Globalization increases with time, and for future economic growth, industry has to adopt low carbon technologies [5][6]. There is some major difference underlined between hydrogen reduction and carbothermic or carbon monoxide reduction from a metallurgical point of view. Iron oxide reduction with hydrogen is endothermic, however, the reduction kinetics is high therefore the industrial operation must be different compared to conventional carbothermic reduction[7]. The reduction of iron oxide by hydrogen goes through either two or three steps depending upon the applied reduction temperature. Temperature higher than 570 °C, hematite ($Fe_2O_3$) transforms to magnetite($Fe_3O_4$) and wustite (FeO) and finally to metallic iron but at temperatures below 570 °C, hematite($Fe_2O_3$) to magnetite($Fe_3O_4$) first, and then directly to metallic iron because wustite (FeO) is not stable below 570 °C [7] [8].

Limited research works have been carried out in literature on the hydrogen reduction of BR and bauxite ore. Low temperature Hydrogen reduction of BR has been studied for the conversion of $Fe_2O_3$ to $Fe_3O_4$ and formation of leachable sodium aluminate phase [9]. They found the maximum conversion of hematite to magnetite around 96 % with 20 wt % NaOH addition and reduction with 5 vol% $H_2$ for 120 mins at 500 °C. Hydrogen reduction of Bauxite ore has been studied [3] for the iron separation prior the ore smelting. It was found that the reduction of Hematite to iron starts below 560 °C and the rate and extent of reduction increases with increasing temperature, however, formation of hercynite ($FeAl_2O_4$) retards the complete reduction above 760 °C. The addition of sufficient Ca to BR avoids the hercynite formation during the reduction step.

This work focuses on hydrogen reduction behaviour of BR pellets, phases formation in the process and mechanical properties of two different types of pellets with similar reduction conditions. $CaCO_3$ is partly substituted by CaO in order to make self-hardening pellets that do not need to be sintered before a reduction in hydrogen thereby reducing the cost of the process. The effect of CaO addition on the pellets strength and the phase formation have been studied. The mechanical properties are studied through breaking load test, tumbler test, and abrasion test for the sintered and self-hardened pellets, and it is shown that they are related to the type of pellets, in addition to the chemical and physical properties of the pellets

## 2. Experimental Procedure/ Research Methodology

### 2.1 Materials

Bauxite residue (BR), limestone (CaCO3), quick lime (CaO), and water were used for pellet making. BR was supplied from the Mytilineos metallurgy business unit S.A. (previously known as aluminum of Greece). The limestone was provided by VUGIUKLI SA, Greece, and quick lime was from the NorFraKalk. The materials were deagglometered and sieved below 500 μm and dried in oven for overnight at 80 °C. Before pelletization, the dried materials with the appropriate ratio were mixed well for homogenization.

### 2.2 Pellets Making

For the self-hardened pellets,1000g of BR, 497 g of limestone, and 80 g of quicklime were mixed in a rotating drum with clockwise and anti-clockwise rotation for 4 minutes for homogenization, but in sintered pellets only 639 g $CaCO_3$ used per 1000 g of BR. However, in both mixtures the calcium weight fraction remains fixed ($CaO/Al_2O_3 = 1$) regarding the chemical compositions of BR, Limestone and quick lime presented in Table1.

**Table1. Chemical composition of BR, Limestone, and quicklime (wt%).**

| | BR | Limestone | Quick Lime |
|---|---|---|---|
| $Al_2O_3$ | 22 | 0.9 | 0.24 |
| CaO | 8.8 | 52.7 | 96.7 |
| $Fe_2O_3$ | 40.71 | 0.15 | 0.08 |
| $K_2O$ | 0.09 | 0.12 | …. |
| MnO | 0.08 | …. | …. |
| MgO | 0.23 | 0.95 | 0.64 |
| $Na_2O$ | 3.1 | …. | …. |
| $P_2O_5$ | 0.11 | 0.01 | 0.02 |
| $SO_3$ | 0.95 | 0.06 | …. |
| $SiO_2$ | 7.1 | 2.07 | 0.46 |
| $TiO_2$ | 5 | 0.03 | 0.02 |
| LOI | 12.4 | 42.6 | 0.5 |

The homogenized mixture was used for the pelletization process in a lab scale drum pelletizer with a stirrer of 80 mm and the rotation 300 rpm speed for 15 minutes. But in sintered pellets, BR and limestone were first mixed in a ball mill and the mixed materials were pelletized in a disk pelletizer with 45-degree rotation angle and 25 rpm via the addition of water. The water addition is the same for both types of pellets which are about 10 wt %. Second group green pellets were dried overnight at 80 °C, and the dried pellets were sintered at about 1150 ±10 °C in muffle furnace within 120 minutes and furnace cooled. For Both pellets size was about 4 to 10 mm. In this work, we used two nomenclatures for the two pellets first is “self-hardened pellet” and second one is “sintered pellet”.

### 2.3 Characterization and Mechanical Properties

The mineralogical phase analysis of materials was done by using X-ray Diffraction (XRD) using Bruker D8 A25 DaVinciTM, Karlsruhe, Germany with the CuKα radiation in 2θ range from 15 to 75 degree diffraction wavelength with step size 0.03 degree. The chemical composition of the material was determined by using X-ray fluorescence (XRF) supplied by Thermo Fisher, Degerfors lab AB, Sweden. Microstructural analysis of the treated material was done by a scanning electron microscope (SEM) supplied by Zeiss ultra 55LE, Carl Zeiss. Jena, Germany. The elemental distribution was assessed using elemental mapping via Energy Dispersive spectroscopy (EDS), Bruker AXS, microanalysis GmbH, Berlin, Germany.

To determine the strength of the pellets we used a compact hydraulic press. Three measurements for each pellet were done and take the average for the calculation of the breaking load. Tumbler and abrasion tests were done as per international standard ISO 3271,3rd edition[10].For the tumbler and abrasion test we used pellets of size greater than 7mm diameter in a mini-tumbler test unit in which a standard [10] is re-scaled to smaller size. The dimension of tumbler was 200 mm inner diameter, 12 mm length and four lifters with height of 6mm. Abrasion index calculated based on the weight fraction of fines below 500 µm divided the total weight pellets. Tumble Index was calculated as the weight fraction above 5.5 mm pellets divided by the total weight of the pellets taken for the testing.

### 2.4 Hydrogen Reduction of Pellets

Direct reduction of both type of the pellets by hydrogen gas was carried out in a thermogravimetry furnace. The setup of the furnace is shown in the Figure 1 below; the crucible schematic (1A), and the whole furnace setup (1B). A thermocouple was inserted in the middle of the crucible to measure the temperature of the sample. The pellets were heated at the rate of 10 °C/min to

1000 ± 5 °C with argon purging 1 Nl/min, and after the reduction step, sample cooling was also with the same flow rate of argon. In the reduction step the argon purging was changed to only hydrogen with a flow rate of 4 Nl/min for about 90 minutes.

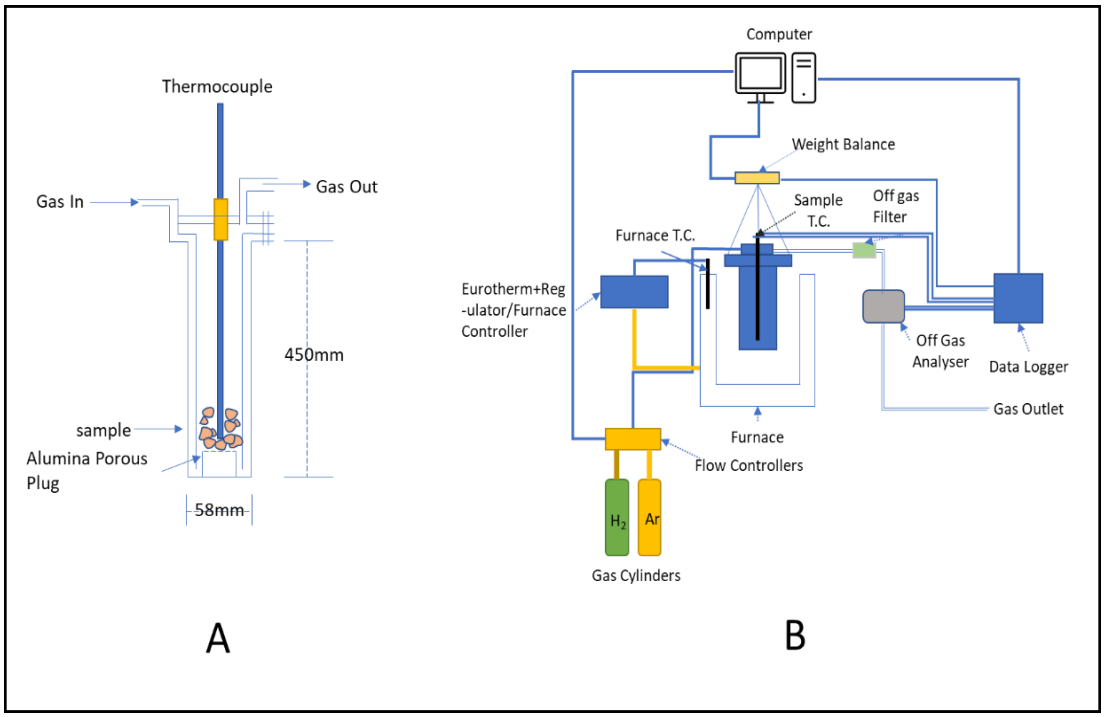


**Figure 1. Schematic view of crucible (A), and the overall furnace setup (B).**

## 3. Results

### 3.1 Phase Analysis

Iron is present in the BR mostly as hematite ($Fe_2O_3$) and goethite ($FeHO_2$). Aluminium is present in many phases such as diaspore ($AlHO_2$), cancrinite($C_{0.76}H_{1.7}Al_3Ca_{0.75}Na_3O_{14.4}Si_3$), katoite ($AlCa_3H_{9.7}O_{12}Si_{0.69}$), and sodalite ($Al_3ClNa_4O_{12}Si_3$). Other than these phases the BR also contained perovskite ($CaTiO_3$), coesite ($SiO_2$), anatase ($TiO_2$), and calcite ($CaCO_3$). Limestone is mainly composed of calcite ($CaCO_3$), which is shown in the XRD (Figure. 2) and XRF (Table 1) results.

XRD spectrums of both reduced pellets are shown in Figure 2. The metallic iron in the reduced sintered pellets has higher intensity as compared to the reduced self-hardened pellets.

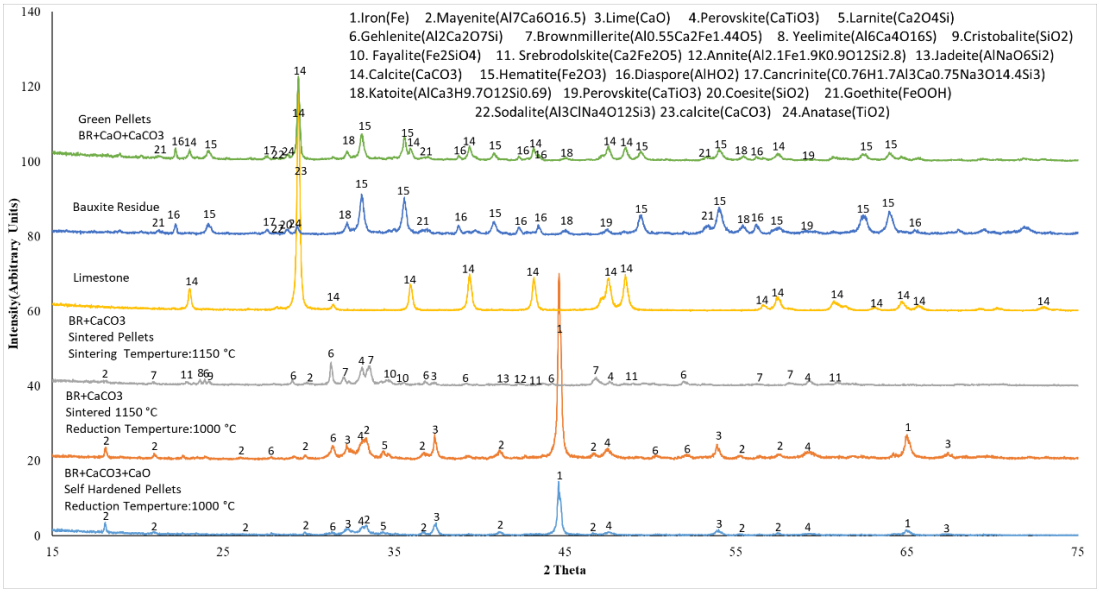


**Figure 2. XRD Spectrum of BR, limestone, green self-hardened Pellet, sintered Pellet, reduced self-hardened pellet and reduced sintered pellet.**

It can be seen in Figure 2 that in the reduced self-hardened pellets, there is much lower amount of gehlenite ($Ca_2Al_2SiO_7$) compared to that in the reduced sintered pellet. Reduced self-hardened pellet had higher intensity of mayenite ($Ca_{12}Al_{14}O_{33}$) compared to that in reduced sintered pellet. The calcium oxide (CaO) had a much higher intensity spectrum in the reduced sintered pellet as compared to self-hardened reduced pellet. In the green self-hardened pellets, all the calcium present is in calcite ($CaCO_3$) form.

### 3.2 Microstructural Analysis

As per the SEM image (Figure 3), there is more clustering of metallic iron particle in reduced self-hardened pellets as compared to reduced sintered pellets. In reduced sintered pellet the iron particle size is smaller and distributed all over the matrix shown in Figure 3a. $CaTiO_3$ is shown in both reduced pellets and $Ca_2Al_2SiO_7$ only in reduced sintered pellets shown in Figure 3a.

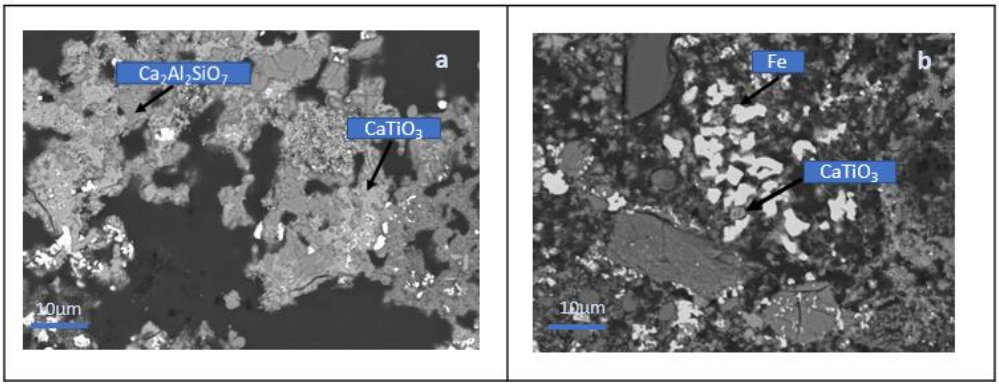


**Figure 3. SEM image of the reduced sintered(a) and reduced self-hardened pellets(b).**

Figures 4a and 4b show the EDS elemental mapping for the two reduced pellets. In the reduced sintered pellet, Ca, Al, and Si have association, which is most likely the gehlenite phase, but that phase is not seen in the reduced self-hardened pellet. In both pellets Ca, and Ti present in forms of $CaTiO_3$ according to the X-Ray mapping results, which is correlated with the XRD results.

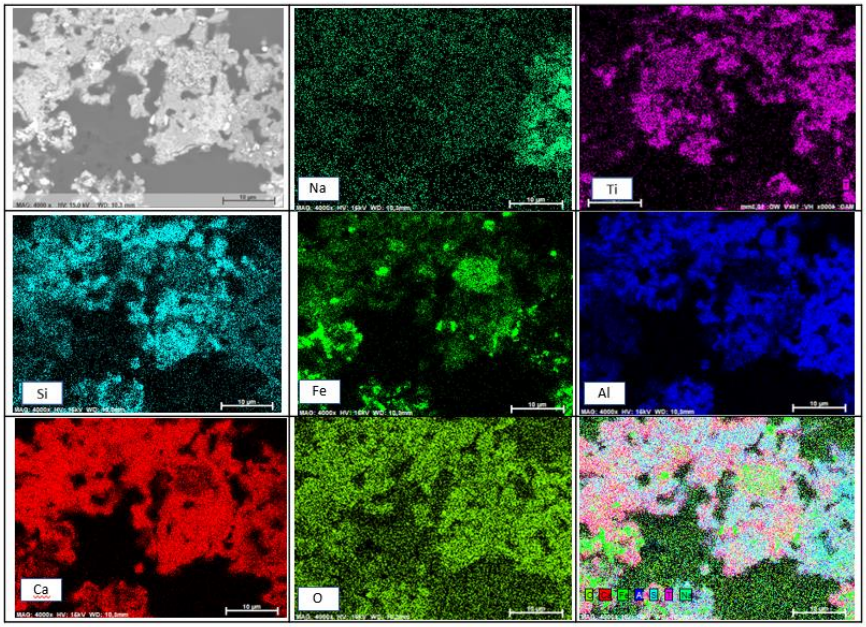


**(a)Reduced sintered Pellet.**

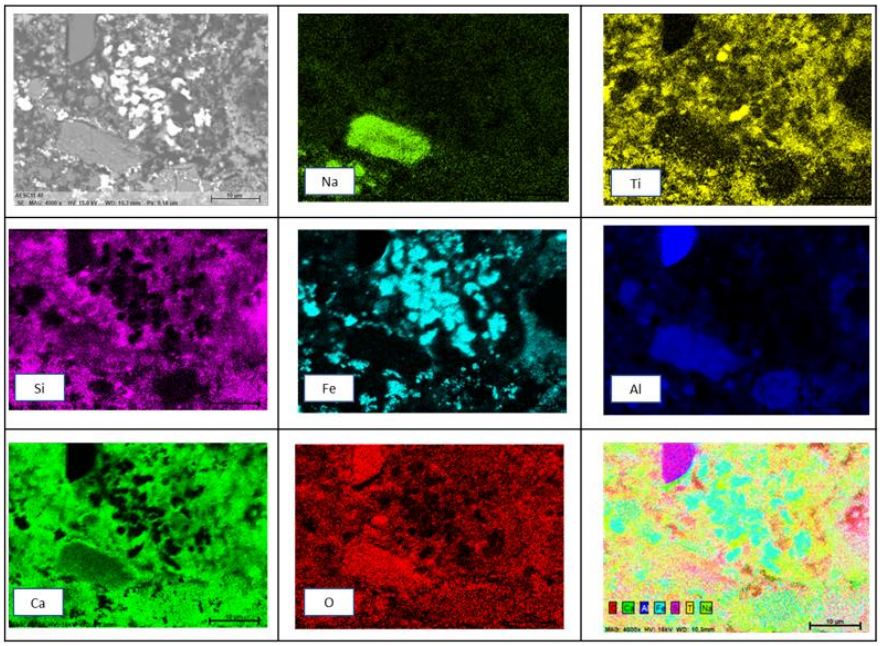


**(b)Reduced self- Hardened pellet**

**Figure 4. Elemental mapping of (a)reduced sintered pellet, and (b) reduced self-hardened pellet.**

### 3.3 Mechanical Properties

Based on the visual observation it was found that the sintered pellet at 1150 °C for 120 minutes had good strength compared to the self-hardened pellet. The measured tumble index is very low for the self-hardened pellet as compared to sintered pellet in Table 2. Good strength of pellets can be evaluated considering the abrasion index below 6 % and tumble index above 92 %[11]. The tumble index is 58.4 % for self-hardened pellets and 88.3 % for the sintered pellets which is shown in Table 2. Lower abrasion index indicates less degradation and dust formation from the pellets

in handling and in the process. Table 2 shows that the self-hardened pellets have the higher abrasion index of 34.5 %, which shows that this pellet is much more susceptible to abrasion. In addition, the breaking load for sintered pellets is more than ten times higher than the self-hardened pellets.

**Table 2. Comparison of mechanical properties of two different pellets.**

| | **Self-Hardened Pellets (BR+CaO+$CaCO_3$)** | **Sintered Pellets (BR+$CaCO_3$),1150 ºC** |
|---|---|---|
| Breaking Load | 0.023 KN (Average of 3 pellets) | 0.29 KN (Average of 3 Pellets) |
| Tumble Index | 58.42 % | 88.33 % |
| Abrasion Index | 34.87 % | 4.89 % |

The measured density for the reduced sintered pellet was around 3.55 g/$cm^3$ and it was around 3.57 g/$cm^3$ for the reduced self-hardened pellet. The measured porosity of the reduced sintered pellet was around 51.74 %, while for the self-hardened reduced pellet was around 68.98 %.

### 3.4 Weight Loss During Hydrogen Reduction

Figure 5 shows the weight changes with respect to the reduction time for two types of pellets. As seen, there is no weight loss for the sintered pellet sample during the heating step in Ar atmosphere but in the self-hardened pellets there is weight loss, which is around 13.13 g out of 51.92 g of the sample. Initially, there is very small weight loss of the self-hardened pellets but after about 40 mins of heating and when temperature is around 400 ℃, there is drastic weight loss, which is shown as onset temperature in Figure 5. Drawing tangents over the mass reduction curve for this pellet gives this temperature. In the reduction regime, when hydrogen is introduced, the mass loss in reduce sintered pellets is around 5.71 g and reduce self-hardened pellets around 4.713 g, which is near to theoretical mass loss for full reduction of iron oxide.

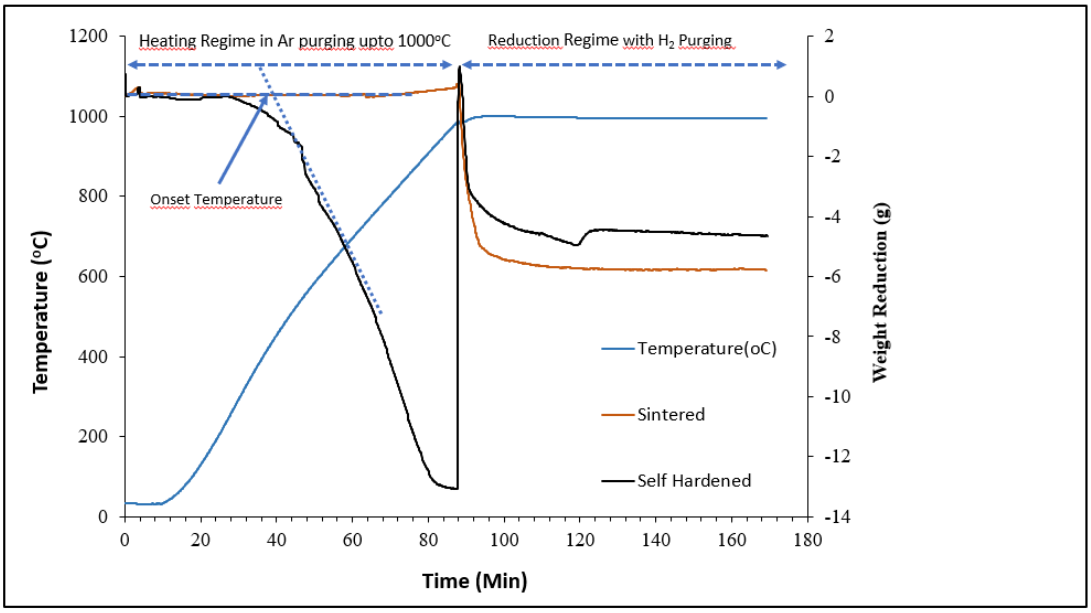


**Figure 5. Weight reduction vs time graphs of sintered and self-hardened pellets.**

## 4. Discussion

The obtained results presented above are discussed as follows.

### 4.1 Mechanical Properties of Oxide Pellets

There is a significant difference between the strength of sintered and self-hardened pellets and the sintered oxide pellet showed better performance. The strength of the dried self-hardened pellets comes from the chemical reaction of quick lime. Quick lime has good plasticity and excellent cementitious property [12] which gives strength to the self-hardened pellets. When quick lime reacts with moisture it forms $Ca(OH)_2$ and the hardening properties of quick lime comes when it reacts with $CO_2$ in air to from $CaCO_3$ which is in accord with the XRD results (Figure 1). The apparent no CaO and $Ca(OH)_2$ in the self-hardened pellet can be taken as a confirmation of the completion of reaction. In order to evaluate the changes, the Gibbs free energy change with temperature for the main reactions were calculated and are plotted in Figure 6. It can be seen that the standard Gibbs energy of formation ($\triangle G^0$) of $Ca(OH)_2$ from CaO and $H_2O$ and then the formation of $CaCO_3$ from $Ca(OH)_2$ at 25 ºC are both negative and hence the reactions occur from thermodynamics point of view. As the $CO_2$ partial pressure in air is low (about 0.06 atm), the changes in Gibbs free energy of formation($\triangle G$) of $CaCO_3$ at 25°C and 0.06 partial pressure of $CO_2$ were also calculated, and the negative values (Figure 6) indicate that the reaction can proceed in pellets in exposure to air. Formation of $Ca(OH)_2$, $CaCO_3$(1atm) and $CaCO_3$(0.06atm) are negative at room temperature and free energy becomes less negative with rise in temperature.

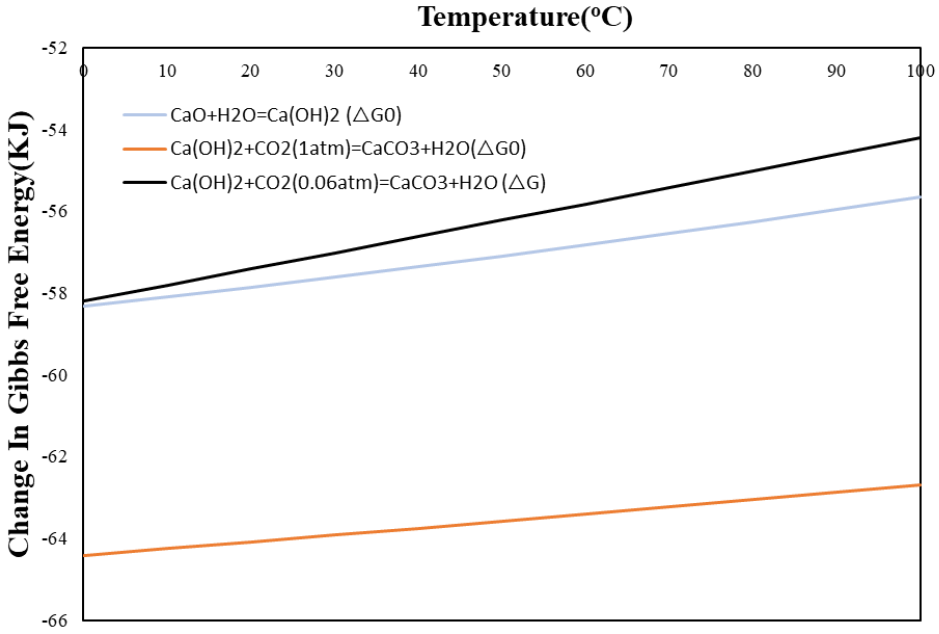


**Figure 6. Gibbs Free energy changes for the formation of $Ca(OH)_2$(1atm), $CaCO_3$(1atm $CO_2$) and $CaCO_3$ (0.06atm $CO_2$);calculated by HSC chemistry 9.**

The porosity of the self-hardened reduced pellets is significantly higher than the sintered pellets due to sintering of pellet components at elevated temperatures. In sintering, surface or partial fusion of particles occur which results in the decreasing porosity of the pellets. In addition, for making the self-hardened pellets $CaCO_3$ was added and CaO, the chemical and thermal behaviour of these species affect the pellet porosity during the heating and reduction steps. Here both hydration of quick lime and carbonation of $Ca(OH)_2$ to $CaCO_3$ have volume expansion[13][14], which results in increases in porosity.

### 4.2 Evolution of Phases during Sintering and Reduction

During the reduction of the self-hardened pellets, there is very little formation of the gehlenite ($Ca_2Al_2SiO_7$) phase as compared to reduced sintered pellets. For the sintered pellet, during sintering the free calcium oxide (formed via $CaCO_3$ decomposition) reacts with adjacent alumina and silica in the BR to form $Ca_2Al_2SiO_7$. Moreover, CaO reacts with alumina and iron oxides to form the brownmillerite ($Ca_2(Fe,Al)_2O_5$) phase. The formation of these phases is confirmed with regard to the sintered oxide pellet XRD spectrum (Figure 2) and microstructural analysis results presented above. According to XRD result of the corresponding reduced sample, the formed brownmillerite ($Ca_2(Fe,Al)_2O_5$) phase in the reduction step is converted to metallic iron, mayenite ($Ca_{12}Al_{14}O_{33}$) and CaO, which is presented via equation 1.The stoichiometry of the equation 1 depends upon the atomic fraction of Fe and Al in $Ca_2(Fe,Al)_2O_5$. In case of self-hardened pellet, the $Fe_2O_3$ in the pellet (originated from BR) is directly reduced to metallic iron via chemical equation 2. In parallel, calcium oxide and alumina in the pellet reacts and yields $Ca_{12}Al_{14}O_{33}$ phase. Both reactant and product phases are confirmed by XRD (Figure 1) for both pellets.

Reduction reaction of sinter pellet:

$$7Ca_2[Fe_x, Al_{1-x}]_2O_5(s) + 21x\ H_2(g) = 14x\ Fe(s) + 21xH_2O(g) + (2 + 12x)CaO(s) + (1 - x)Ca_{12}Al_{14}O_{33}\ (s) \quad (1)$$

Reduction reaction of self-hardened Pellets

$$Fe_2O_3(s) + H_2(g) \rightarrow Fe(s) + H_2O(g) \quad (2)$$

Maybe due to the direct formation of mayenite ($Ca_{12}Al_{14}O_{33}$) phase the amount of the ($Ca_{12}Al_{14}O_{33}$) in the reduced self-hardened pellet is a little more than that in the reduced sintered pellet. In the reduced sintered pellets, some amount of alumina is lost in the $Ca_2Al_2SiO_7$ phase, but in the self-hardened pellets, the free alumina is there for the formation of the $Ca_{12}Al_{14}O_{33}$ phase. Larnite ($Ca_2SiO_4$) phase was found in both reduced samples, which is a dicalcium silicate compound and it shows the interaction of added lime with the $SiO_2$ in BR via the following reaction:

$$2CaO(s) + SiO_2(s) \rightarrow Ca_2SiO_4\ (s) \quad (3)$$

Perovskite ($CaTiO_3$) had the higher intensity in the reduced sintered pellets as compared to reduced self-hardened pellets (Figure 2). This may be due to the high temperature sintering that leads to more interaction of added CaO and $TiO_2$ in BR and formation of $CaTiO_3$, which is a very stable phase.

### 4.3 Mass Changes during Reduction

During the calcination and reduction of self-hardened pellets, there is approximately 13 g of mass loss during heating cycle, which is due to the $CaCO_3$ decomposition, aluminium hydroxide decomposition, goethite (FeO(OH)) decomposition and chemisorbed water. As per mass balance, the $CO_2$ amount from decomposition is near around 7.8 g. Observing the extra mass loss is due to the decomposition of alumina hydroxides compounds and goethite. In the case of heating the sintered and self-hardened pellets in TGA test, there is a little mass increase during the heating which may be due to the argon gas molecules adsorption on the low-energy sites of the porous pellets with high surface area. As shown in the Figure 7 the fraction reduction vs time, iron complex reduction to metallic iron is almost completed, which is also corelated with the theoretical mass loss and actual mass loss during reduction step. Both curves show that fraction reduction goes above 90 % within a short reduction time. The mass balance of iron complex reduction to iron is shown in the Table 3. Fraction reduction is calculated based on equation (4):

$$Fraction\ Reduction(X) = \frac{Actual\ weight\ loss\ (\triangle W_{red})}{Mass\ of\ oxygen\ present\ in\ Fe_2O_3\ (W_{in})} \quad (4)$$

Where $\triangle W_{red}$ is the weight loss during reduction as measured in the reduction and $W_{in}$ is the possible removable oxygen via the reduction.

**Table 3. Comparison of weight loss during reduction of two different pellets.**

| | %$Fe_2O_3$(g) in Initial Mass | Theoretical Mass Loss(g) | Actual Mass Loss (g) |
|---|---|---|---|
| Self-Hardened Pellets | 15.8 | 4.74 | 4.71 |
| Sintered Pellets | 19.1 | 5.73 | 5.71 |

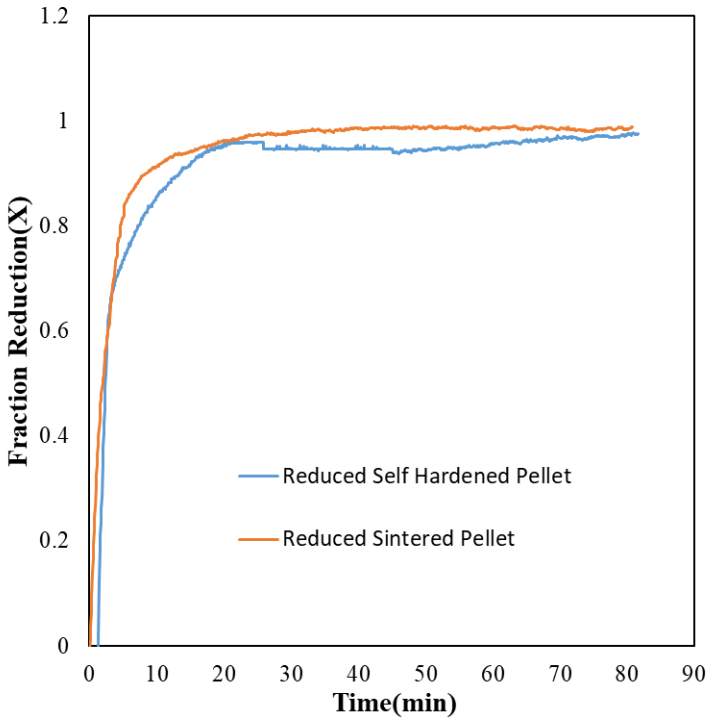


**Figure 7. Fraction reduction of iron complex to metallic iron at 1000°C in $H_2$ atmosphere.**

Observing close X-t behaviour during the $H_2$ reduction of the pellets in Figure 7 may indicate that the mass transport of hydrogen into the two pellets with different porosities is not a rate determining step. Moreover, the reduction of brownmillerite and hematite as the main Fe-containing compounds in the two pellets occurs with high rate.

## 5. Conclusion

Mechanical, chemical, and physical, and structural properties of sintered and self-hardened BR pellets via addition of CaO and $CaCO_3$ were studied. Moreover, isothermal hydrogen reduction of these pellets was studied experimentally. The following main conclusions were obtained.

1. Breaking load, Tumble index and abrasion index of self-hardened pellets is lower than sintered pellets
2. There is negligible amount of gehlenite phase formation during reduction of self-hardened pellets as compared to sintered pellets
3. The intensity of metallic iron is more in reduced sintered pellets as compared to self-hardened pellets

4. Reduction rate and extent of iron containing oxides are very similar for both pellets
5. There is more formation of alumina leachable phase in reduced self-hardened pellets as compared to reduced sintered pellets
6. Iron particle size of reduced self-hardened pellets is more than the reduced sintered pellets

**Acknowledgements**

This project has received funding from the European Union's Horizon 2020 research and innovation programme under grant agreement No 958307. This publication represents only the authors' views, exempting the Community from any liability. The Harare Project website is https://h2020harare.eu/

## 6. References

1. E. A. Association, "The aluminium automotive manual," *Join. Dissimilar Mater.*, pp. 1–31, 2015.
2. J. Safarian and L. Kolbeinsen, "Sustainability in alumina production from bauxite," *Sustain. Ind. Process. Summit*, pp. 75–82, 2016.
3. A. Lazou, C. van der Eijk, E. Balomenos, L. Kolbeinsen, and J. Safarian, "On the Direct Reduction Phenomena of Bauxite Ore Using H 2 Gas in a Fixed Bed Reactor," *J. Sustain. Metall.*, vol. 6, no. 2, pp. 227–238, 2020.
4. H. Baolin, H. Zhang, L. I. Hongzhong, and Z. H. U. Qingshan, "Study on kinetics of iron oxide reduction by hydrogen," *Chinese J. Chem. Eng.*, vol. 20, no. 1, pp. 10–17, 2012.
5. A. Elshkaki, T. E. Graedel, L. Ciacci, and B. K. Reck, "Resource demand scenarios for the major metals," *Environ. Sci. Technol.*, vol. 52, no. 5, pp. 2491–2497, 2018.
6. J. Lee et al., "Reviewing the material and metal security of low-carbon energy transitions," *Renew. Sustain. Energy Rev.*, vol. 124, p. 109789, 2020.
7. D. Wagner, O. Devisme, F. Patisson, and D. Ablitzer, "A laboratory study of the reduction of iron oxides by hydrogen," *arXiv Prepr.* arXiv0803.2831, 2008.
8. W. K. Jozwiak, E. Kaczmarek, T. P. Maniecki, W. Ignaczak, and W. Maniukiewicz, "Reduction behavior of iron oxides in hydrogen and carbon monoxide atmospheres," *Appl. Catal. A Gen.*, vol. 326, no. 1, pp. 17–27, 2007.
9. G. Pilla, S. V Kapelari, T. Hertel, B. Blanpain, and Y. Pontikes, "Hydrogen reduction of bauxite residue and selective metal recovery," *Mater. Today* Proc., vol. 57, pp. 705–710, 2022.
10. ISO, "INTERNATIONAL STANDARD iTeh STANDARD iTeh STANDARD PREVIEW," *Int. Organ. Stand.*, vol. 10406–1:20, pp. 3–6, 2015.
11. B. E. Monsen, E. S. Thomassen, I. Bragstad, E. Ringdalen, and P. H. Hoegaas, "Characterization of DR Pellets for DRI Applications," Conference: AISTech 2015 Proceedings.
12. L. D. Hekmat, "Lecture ( 6 )," pp. 1–6.
13. K. You, H. Jeong, and W. Hyung, "Effects of accelerated carbonation on physical properties of mortar," *J. Asian Archit. Build. Eng.*, vol. 13, no. 1, pp. 217–221, 2014.
14. J. Blamey, M. Zhao, V. Manovic, E. J. Anthony, D. R. Dugwell, and P. S. Fennell, "A shrinking core model for steam hydration of CaO-based sorbents cycled for CO2 capture," *Chem. Eng. J.*, vol. 291, pp. 298–305, 2016.